Giant Enhancement of Excitonic Electro-optic Response in Trap-Reduced Organic Transistors

Satoshi Matsuoka,[1,*] Jun'ya Tsutsumi,[2] and Tatsuo Hasegawa[1]

[1] *Department of Applied Physics, The University of Tokyo, Tokyo, 113-8656, Japan*

[2] *Research Institute for Advanced Electronics and Photonics (RIAEP), National Institute of Advanced Industrial Science and Technology (AIST), Tsukuba, 305-8565, Japan*

(Received 13 March 2021; revised 23 August 2021; accepted 29 September 2021; published 22 October 2021)

Organic field-effect transistors (FETs) exhibit excellent switching characteristics when they involve trap-eliminated semiconductor interfaces with highly hydrophobic gate dielectric layers. In this study, we investigate the excitonic electro-optic response by delocalized carrier accumulation at the trap-eliminated interfaces of pentacene single-crystal FETs. We find that gate-modulation (GM) imaging, which sensitively visualizes the variation in optical microscope images between the gate-*on* and gate-*off* states, exclusively reveals the unique enhancement of electro-optic response under the application of drain voltages (V_d). The V_d-unbiased GM image exhibits a uniform spatial distribution, which is consistent with the accumulated carrier density in the channel. In contrast, the V_d-biased GM image presents a peculiar spatial distribution with fairly sharp increases around the edges of the source and drain electrodes. Furthermore, the following intriguing features are observed: (1) The sharp increase in the GM signal distribution around the electrode edge is similar to the lateral electric field distribution as measured by Kelvin probe force microscopy, and (2) the GM spectra, extracted from the respective GM images measured at different wavelengths, present a second-derivative-like shape that implies the broadening of exciton absorption. Based on these observations, we investigate the origin of this unique effect in terms of the enhanced violation of exciton coherence by delocalized carrier accumulations under drain bias. The gate-induced holes that are weakly bound to shallow traps should be detrapped by lateral electric fields, which eventually generate valence band holes and thus enhance the electro-optic response. These findings should elucidate the spatial coherence of the molecular excitons that are responsible for the various unique photoelectric characteristics of organic electronic devices.

DOI: 10.1103/PhysRevApplied.16.044043

I. INTRODUCTION

The absorption band of small-molecule organic semiconductors (OSCs) in the visible range originates, in most cases, from molecular (or Frenkel) excitons associated with the lowest electronic excitation of intramolecular π-conjugated electronic systems [1,2]. The unique nature of molecular excitons in crystalline OSCs is that the electron-hole relative motion is confined (or localized) to the respective molecules, whereas the exciton wavefunctions are coherently extended over the entire crystal through intermolecular Coulomb interactions and concomitant exciton band formation. When charge carriers are injected and accommodated in OSCs, the excitonic optical responses should undergo a unique variation. Charge-modulation spectroscopy (CMS) based on field-effect transistor (FET) device structures is known to be a unique method for probing tiny changes in exciton absorption spectra caused by gate-induced charge carrier accumulations [3–9]. However, despite the high usability of CMS, the spectral features of several small-molecule OSCs are often complicated and not well understood; this is because of the bleaching [3–5,9], energy shift [6–8], or splitting [5,6,9] of the original exciton absorption.

Recently, an innovative technique, referred to as gate-modulation (GM) imaging, has been developed to obtain spatially resolved electro-optic responses of channel OSC layers via highly sensitive and collective sensing of difference optical microscope images between the gate-*on* and gate-*off* states [10–15]. Using this imaging technique, it was reported that the microscopic GM signals of pentacene polycrystalline thin films exhibit a markedly inhomogeneous spatial distribution, including drastic sign changes over the intragrain and grain boundaries [16,17]. The observed spectral features could be ascribed to inhomogeneous trap distributions between the inside and boundary of the grains. The results indicate that the rather complicated spectral features of the usual CMS, as stated above,

*matsuoka-s@ap.t.u-tokyo.ac.jp

originate from such spatially inhomogeneous GM signals. However, it is not yet clear how the trap density affects the variation of the excitonic electro-optic response of molecular semiconductors by charge accumulation. The issue is of fundamental and critical importance, as it is closely associated with the effect of the spatial coherence of molecular excitons on the unique photoelectric characteristics of organic electronic devices.

In this study, we report that an unexpectedly large excitonic electro-optic response is observed using clean and trap-eliminated single-crystal semiconductor interfaces of pentacene. We utilize the most hydrophobic amorphous perfluoropolymer, Cytop, as the gate dielectric. Notably, Cytop has recently been reported to provide organic FETs with excellent switching characteristics at low operational voltages owing to the elimination of interfacial carrier trap states [18,19]. In particular, we find that the variation in exciton absorption is considerably enhanced by the multiple application of gate and drain potentials in single-crystal devices. We discuss the origin of the enhanced excitonic response in terms of the effects of both delocalized carrier accumulation and lateral field application on molecular excitons that have extended the spatial coherence of wave functions at the OSC interfaces.

II. EXPERIMENT

High-quality flake-like pentacene single crystals are grown by the physical vapor transport (PVT) technique, as schematically depicted in Fig. 1(a) [20–22]. The growth is achieved with a source temperature of 560 K and N_2 gas flow of 30 cm^3 min^{-1} for 10 h. In the device fabrication, a Cytop layer with a thickness of either 250 or 400 nm is fabricated on semi-transparent substrates composed of quartz glass and an ultrathin gold gate electrode with a thickness of 6 nm. After the gold source and drain electrodes are formed, the pentacene singe crystals are laminated on top of the Cytop layer, as seen in Fig. 1(b). The obtained device exhibits a sharp switching characteristic from approximately 0 V, with a small subthreshold swing (SS) value of 0.2 V dec^{-1}, mobility of 1.0 cm^2 V^{-1} s^{-1}, and negligible hysteresis [23,24]. The small SS value is ascribed to the low interfacial trap density associated with both the low surface free energy and the low bulk permittivity [18,25].

The GM imaging measurements are conducted with a home-assembled apparatus of an optical microscope and a highly sensitive CMOS area image sensor. The FET devices are irradiated with monochromatic light from a halogen light source. The transmitted optical images are captured by the CMOS sensor in synchronization with the square-wave modulated gate bias alternating between 0 V (gate-*off* state) and −80 V (gate-*on* state) at 40 Hz. We obtain the GM images from the difference image between these states. The states are presented with respect to $\Delta T/T$, where T and ΔT are the optical transmittance of the device and variation of the transmittance owing to the modulated gate bias in each pixel, respectively. The obtained GM images are integrated 2^{14} (=16 384) times to reduce noise and visualize the GM signal clearly.

As a reference device, we manufacture polymer FETs based on the typical donor-acceptor-type copolymer, poly{3,6-dithiophen-2-yl-2,5-di(2-decyltetradecyl) -pyrrolo[3,4-c]pyrrole-1,4-dione-alt-hienylenevinylene-2, 5-yl} (PDVT-10) [26]. We use the same semitransparent substrates composed of a Cytop gate dielectric layer, as mentioned previously. The semiconductor channel layer is coated using the push coating technique [27]. The device exhibits excellent transfer characteristics with a mobility of 0.3 cm^2 V^{-1} s^{-1} and negligible hysteresis.

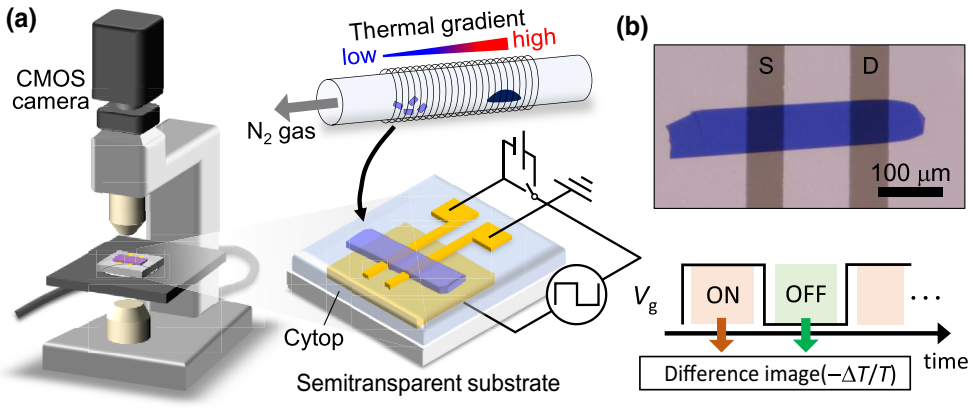

FIG. 1. (a) Schematic of a setup of GM imaging measurements, the furnace of the PVT, and a single-crystal FET, which is composed of a Cytop gate dielectric, which are used for the GM imaging measurements. (b) An optical micrograph of a pentacene signal-crystal FET with source (S) and drain (D) electrodes.

III. RESULTS AND DISCUSSION

A. Enhancement of GM signal under drain fields

Figure 2 presents the GM images of a pentacene single-crystal FET obtained at a wavelength of 670 nm (photon energy of 1.85 eV), which roughly corresponds to the peak energy of exciton absorption [28,29]. The device exhibits a rather uniform spatial distribution of the GM signal ($\Delta T/T \sim 1 \times 10^{-3}$, blue-colored) over the entire channel, with a clear step rise at the electrode edge, when the drain field is not applied (i.e., the drain potential is the same as the source potential). The sign of the observed GM signal is positive, indicating an increase in transmittance, and the signal intensity is proportional to the modulated gate bias (or the accumulated carrier density), as seen in Fig. 3(d). The results indicate that a decrease in exciton absorption is ascribed to charge accumulation within the channels.

The most intriguing observation is that the device exhibits an enhanced GM signal owing to the application of the drain bias, as presented in Fig. 2(c). The GM signal intensity under the drain bias is approximately 5 times larger than that without the drain bias. Notably, these observations are contradictory to the naive presumption that the GM signal should be proportional to the accumulated carrier density: according to the general understanding of FET operation, the total number of charge carriers under the drain bias should be smaller than that without the drain bias. The carrier density under the saturation regime should decrease almost linearly with the distance from the source electrode edge (as expressed by the gradual channel approximation) and should be completely depleted at the pinch-off point near the drain electrode edge. Thus, the enhanced GM signal is not consistent with the pure concept of carrier accumulation within the channels.

The observed GM image also presents a peculiar spatial distribution of the GM signal within the channel: the signal exhibits fairly sharp increases at both electrode edges; further, it increases gradually from the source to the drain. When the source and drain electrodes are interchanged, the above profile is clearly reversed with regard to the center of the channel. We also notice that on the source and drain electrodes, the GM signal distribution exhibits a tail-like decay with increasing distance from the channel in both directions, although no GM signal is observed on the

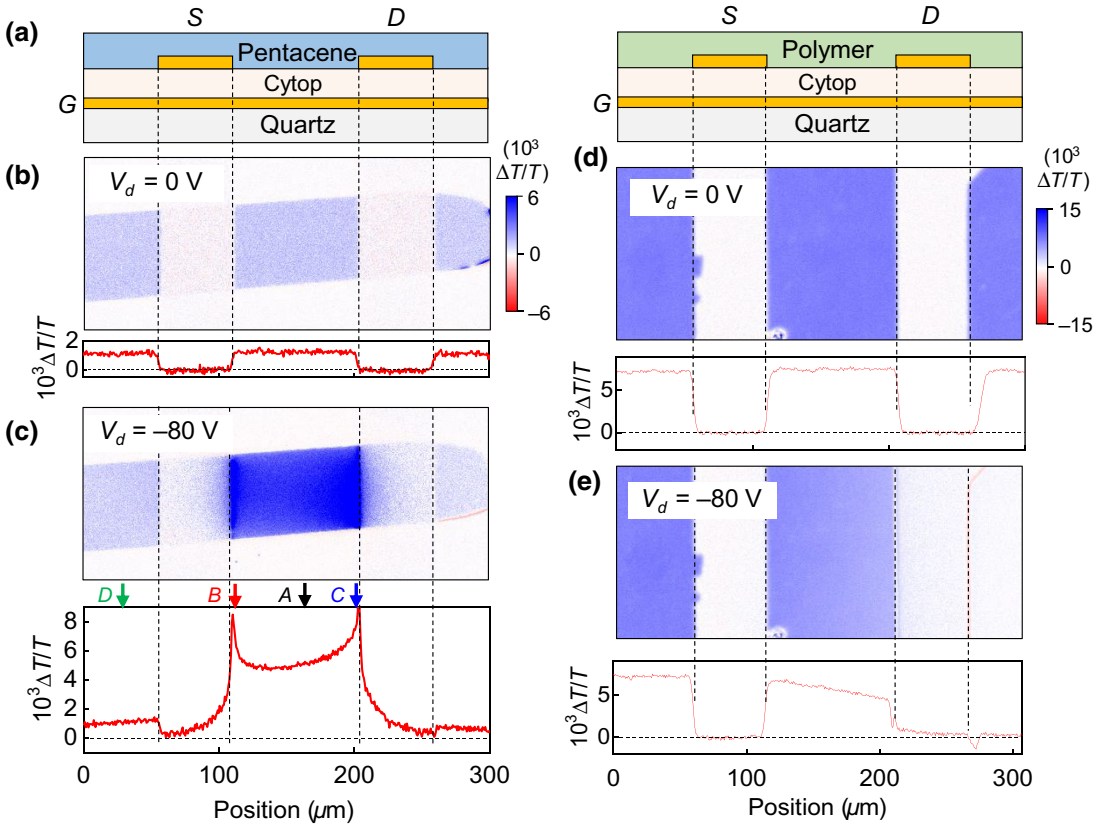

FIG. 2. (a) Cross-section schematics of pentacene (left) and polymer (right) FETs with source (S), drain (D) and gate (G) electrodes, used for GM imaging measurements. (b)–(e) Microscope GM images of the pentacene single-crystal FET (b) and (c) and the PDVT-10 FET (d) and (e), obtained with a modulated gate bias at $V_{g\,\mathrm{mod}} = -80$ V without drain bias (b) and (d) and with dc drain biases at $V_{d\,\mathrm{dc}} = -80$ V (c) and (e). Profiles of GM signal distribution along the semiconducting channel layer are extracted from the respective GM images, and are presented in the lower panel of each microscope GM image.

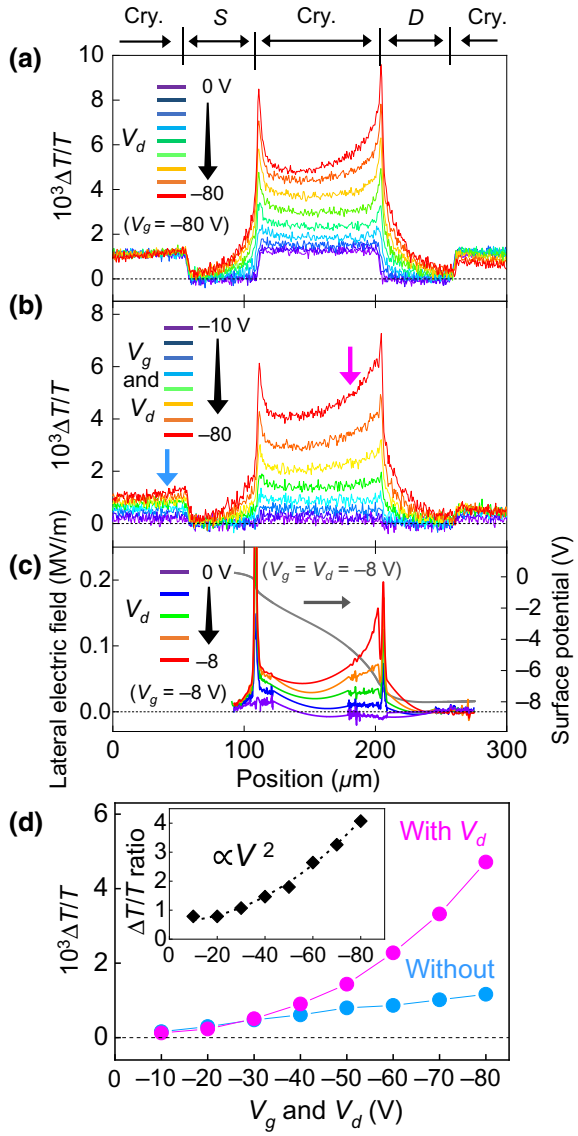

FIG. 3. (a) Bias-dependent GM signal profiles along the crystal channel layer (Cry.) of pentacene single-crystal FET with Cytop gate dielectric layer, measured at different dc drain biases ($V_{d\mathrm{dc}}$ = 0 to −80 V) under the same modulated gate bias ($V_{g\mathrm{mod}}$ = −80 V) and (b) under modulated drain and gate biases ($V_{d\mathrm{mod}}$ = $V_{g\mathrm{mod}}$ = −10 to −80 V). (c) Lateral electric field distributions derived from the spatial differentiation of surface potential (which is shown by a gray curve), measured at different dc drain biases ($V_{d\mathrm{dc}}$ = 0 to −8 V) and at constant dc gate bias ($V_{g\mathrm{dc}}$ = −8 V) by Kelvin probe force microscopy. (d) Variations of GM signal intensity are plotted as a function of modulated gate bias: with modulated drain bias (pink) and without drain bias (light blue) and the ratio between the cases with and without the drain bias (inset).

electrodes without a drain bias. This observation is in contrast to the general assumption that the GM signal should be proportional to the accumulated carrier density because the carrier density should be very small on top of the source and drain electrodes, even with drain biases.

Here, we note that the GM signal is not detectable when the gate voltage is not biased, even if the drain voltage is modulated. This indicates that the pure field modulation (or electroabsorption) signal is much lower than the observed GM signal. Therefore, the observed substantial enhancement of the GM signal under the drain bias is attributable to the effect of biased drain fields on the accumulated charge carriers. Such an enhancement in the electro-optic response, realized by a combined application of drain and gate potentials, has not been reported to date for any material or device. It is important to note that no such enhancement has been observed in pentacene polycrystalline FETs with hydrophilic silicon dioxide gate dielectrics [16,17], or in pentacene single-crystal FETs composed of typical polymer gate dielectrics, such as poly(methylmethacrylate) or cross-linked poly(vinylphenol).

We conduct similar GM imaging measurements for the FET composed of a PDVT-10 channel layer and a Cytop gate dielectric layer. Figures 2(d) and 2(e) present the observed GM images without and with drain bias, respectively. The results are shown for the measurements at a wavelength of 830 nm (photon energy of 1.49 eV), which corresponds to the absorption peak due to HOMO-LUMO excitation. The GM signal distribution without the drain bias is homogeneous over the entire channel, similar to the case of the pentacene single-crystal FET. Meanwhile, no enhancement is observed in the GM response in the case with the drain bias: the GM signal gradually decreases almost linearly with the distance from the source electrode edge to the drain electrode edge, the distribution of which seems to obey the gradual channel approximation of the carrier density within the channel. This result implies that the device with the Cytop gate dielectric layer does not necessarily enhance the GM signal. We consider that the enhancement effect should manifest itself only in the case of highly delocalized carriers accumulated at the trap-eliminated semiconductor-dielectric interfaces.

B. Drain-bias dependent GM signal and lateral field distribution

Figure 3 presents the profiles of GM signal distributions measured at 1.85 eV with different combinations of dc and modulated-ac biases. Note that the GM signal observed outside the source electrode, as shown in Figs. 3(a) and 3(b), can be utilized as a reference GM signal without the drain bias, which is only proportional to the applied modulated gate bias. From the comparisons, the ratio of the GM signals with and without the drain bias is estimated, the result of which is shown in the inset of Fig. 3(d). The ratio shows a clear square dependence on the applied drain bias. Eventually, the GM signal presents a cubic dependence on the modulated bias when the drain and gate are equipotential, and both are used as the modulated bias.

We also conduct Kelvin probe force microscopy measurements [30,31] to investigate the lateral electric field distribution within the channel, the results of which are shown in Fig. 3(c). The strong lateral fields around the electrode edges are due to the large potential drops, either associated with the contact resistance or the pinch-off state around the drain electrode. In particular, the field distribution profile exhibits a fairly sharp rise around the electrode edge, and such features are quite similar to those of the GM signal profile.

C. Spectral analyses of GM signal under drain fields

GM (or CMS) spectra of pentacene single crystals both with and without drain biases are extracted from the respective GM images measured at different wavelengths, the results of which are shown as $-\Delta T/T\,(=\Delta\alpha d$;

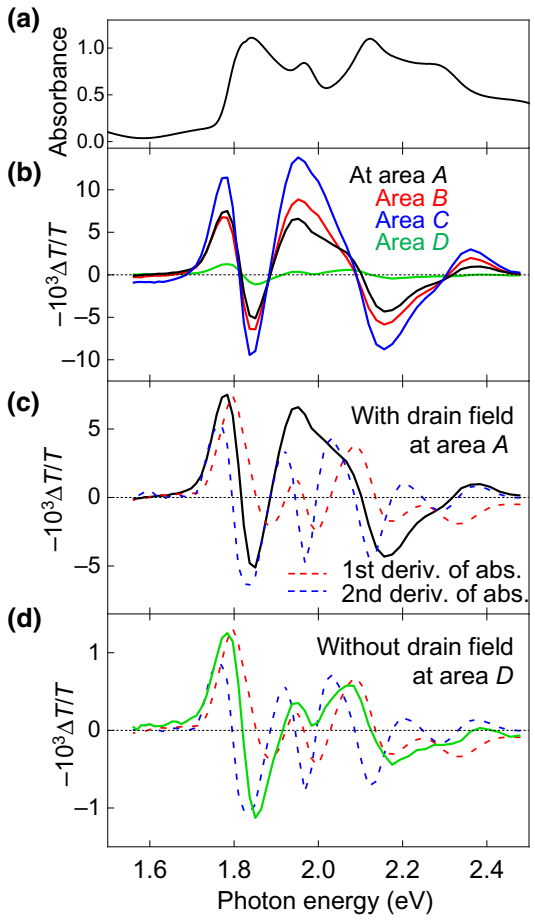

FIG. 4. (a) Optical absorption spectrum and (b) GM spectra measured at different positions with the drain biases [at areas *A*, *B*, and *C*, as depicted in Fig. 2(c)] and without the drain bias (at area *D*), for pentacene single-crystal FETs with Cytop gate dielectric layer. Comparisons of the GM spectra measured (c) with and (d) without drain biases, with the first and second derivatives of the absorption spectrum (red and blue dashed curves, respectively).

variation of absorption coefficient α multiplied by layer thickness d) spectra in Fig. 4. The GM signal is clearly enhanced under the drain bias over the entire photon energy region of the exciton absorption. The spectral features observed around the main exciton absorption peak at 1.7–1.9 eV are quite similar to each other for all the spectra measured at different positions with the drain biases (at areas *A*, *B*, and *C*) and without the drain bias (at area *D*), despite the considerable difference in signal intensity. This feature is roughly consistent with the second derivative of the original exciton absorption spectrum, and can be attributed to the spectral broadening of the exciton absorption owing to carrier injection [9]. By contrast, a distinct difference between the GM (or CMS) spectra obtained with and without the drain bias is observed at the higher energy side, at approximately 1.9–2.1 eV, while the spectral features are roughly common to all the channel positions under the drain bias (at areas *A*, *B*, and *C*). We consider that the spectral feature observed under the drain bias could be ascribed to the generation of free electron-hole pairs, as discussed in the following [32].

D. Origin of enhanced GM signal under drain fields

The square electric field dependence of the electro-optic response, as shown in Fig. 3(d), is frequently observed in electroabsorption measurements, such as the Franz-Keldysh effect [33,34], the Stark effect [6–8] and/or the quantum-confined Stark effect [35–37]. However, the lateral electric field applied in the present device (0.8 MV m^{-1}) is much smaller than the applied electric fields used in the conventional electroabsorption measurements (5.6 MV m^{-1}). Furthermore, the first-derivative-like component due to the Stark shift of the exciton absorption is not observed in the enhanced GM spectra, as evidenced in this study. Thus, it is clear that the enhanced GM signal does not originate from the electroabsorption; rather, it originates from the multiplicative effect, which is only observed by the field application on highly delocalized carriers at semiconductor-dielectric interfaces.

Second-derivative-like CMS spectra, observed around the main exciton absorption, have been reported for highly ordered polymeric semiconductors, including PDVT-10 [9]. It is indicated that the second-derivative-like spectra should originate from the broadening of the original exciton absorption, and should be ascribed to the effect of carrier accumulations for violating the exciton coherence. Thus, the observation of enhanced second-derivative-like CMS spectra under the drain bias indicates that the application of drain potential should be effective in enhancing the effect of accumulated carriers on the exciton coherence over a wider area of channels. As the carriers injected into the channel layers are accommodated at carrier traps located within the channels or channel interfaces in organic FETs, the change in exciton absorption should be ascribed

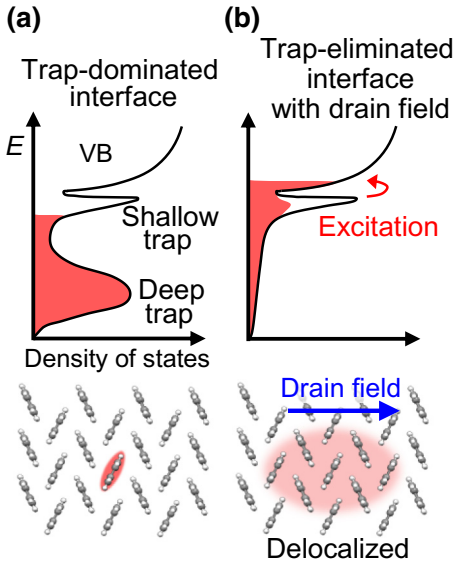

FIG. 5. Schematics for energy (E) distribution of charge carriers near valence band (VB) states (a) in conventional trap-dominated organic FETs, and (b) in trap-eliminated organic FETs under drain bias. Top: Excitation of holes from the shallow trap states to the valence band states owing to the drain field. Bottom: Spatial extensions of carriers within organic crystals in the respective cases.

to the change in exciton coherence around the trapped carriers. These carriers should be delocalized or very weakly localized in trap-eliminated single-crystal FETs composed of Cytop. Therefore, it is reasonable to consider that the lateral electric fields should help to detrap the holes, which are weakly bound to shallow traps, into valence band states that have larger spatial extensions in the crystals, as shown in Fig. 5. In fact, the appearance of spectral features at 1.9–2.1 eV should be closely associated with the enhancement of free electron-hole pair generation within the channels [32]. The generation of holes in the valence bands should increase the effective number of molecules that are affected by the holes, which eventually leads to the enhancement of the GM signal. In this context, we suggest that the observed considerable enhancement effects should be correlated with the giant oscillator strength effect, which is introduced to describe enhanced exciton absorption owing to isotopic impurities with shallow discrete levels near the exciton band [2,38], in which the exciton coherence with spatial extension plays a critical role. Although the detailed enhancement mechanism remains uncertain, the enhancement effect of the GM signal observed in this study is quite intriguing and promising for elucidating the unexplained physical phenomena of the excitonic responses in molecular crystals.

IV. SUMMARY

We observe the unique excitonic electro-optic response of organic semiconductors due to electric field applications on highly delocalized carriers. We utilize trap-eliminated organic FETs composed of fairly clean semiconductor-dielectric interfaces between the most hydrophobic amorphous perfluoropolymer, Cytop, and high-quality flake-like single crystals of pentacene. We find that the GM image, which sensitively visualizes the variation of the optical microscope image between the gate-*on* and gate-*off* states, exhibits a significant signal enhancement and peculiar distribution under the application of the drain voltage (V_d). The V_d-unbiased GM image exhibits a rather uniform spatial distribution over the entire channel, whereas the V_d-biased GM image presents a peculiar spatial distribution whose feature is fundamentally different from the distribution of the accumulated carrier density within the channel. The V_d-biased GM signal distribution exhibits fairly sharp increases at the edges of the source and drain electrodes, a feature which is rather similar to that of the distribution profiles of the lateral electric field, as observed by Kelvin probe force microscopy. No such feature is obtained in the case of semiconducting polymer FETs composed of a Cytop gate dielectric layer.

We assess the origin of the observed unique electro-optic effect in terms of the enhanced violation of exciton coherence by delocalized carrier accumulations. We consider that the enhanced effect under drain bias is associated with the detrapping of holes that are weakly bound to shallow traps, which eventually generate valence band holes. The band holes have larger spatial extensions than the trapped holes; therefore, the detrapping effect should more considerably affect the molecular exciton absorption. In particular, the exciton coherence should be reduced by the delocalized carrier accumulations, which results in the broadening of the exciton absorption. This is consistent with the observed second-derivative-like GM spectra of the main exciton absorption. Such an intriguing enhancement effect in the electro-optic response has not been reported to date for any material or device. We believe that our findings should advance progress in understanding the spatial coherence of the molecular excitons that are responsible for the various unique photoelectric characteristics of organic electronic devices.

ACKNOWLEDGMENTS

This work is supported by the Japan Society for the Promotion of Science (JSPS) KAKENHI (Grants No. JP19K15432, No. JP19H02587, and No. 21H04651) and by the Japan Science and Technology Agency (JPS) CREST (Grant No. JPMJCR18J2).

[1] M. Pope and C. E. Swenberg, *Electronic Processes in Organic Crystals and Polymers*, 2nd ed. (Oxford University Press, Oxford, 1999).

[2] V. L. Broude, E. I. Rashba, and E. F. Sheka, *Spectroscopy of Molecular Excitons*, Softcover reprint of the original 1st ed. (Springer-Verlag, Berlin, Heidelberg, New York, Tokyo, 2012).

[3] K. E. Ziemelis, A. T. Hussain, D. D. C. Bradley, R. H. Friend, J. Rühe, and G. Wegner, Optical Spectroscopy of Field-Induced Charge in Poly(3-Hexyl Thienylene) Metal-Insulator-Semiconductor Structures: Evidence for Polarons, Phys. Rev. Lett. **66**, 2231 (1991).

[4] P. J. Brown, H. Sirringhaus, M. Harrison, M. Shkunov, and R. H. Friend, Optical spectroscopy of field-induced charge in self-organized high mobility poly(3-hexylthiophene), Phys. Rev. B **63**, 125204 (2001).

[5] T. Sakanoue and H. Sirringhaus, Band-like temperature dependence of mobility in a solution-processed organic semiconductor, Nat. Mater. **9**, 736 (2010).

[6] S. Haas, H. Matsui, and T. Hasegawa, Field-modulation spectroscopy of pentacene thin films using field-effect devices: Reconsideration of the excitonic structure, Phys. Rev. B **82**, 161301(R) (2010).

[7] Y. Harima, Y. Ishiguro, K. Komaguchi, I. Imae, and Y. Ooyama, Optical absorption spectrum of pentacene cation radicals measured by charge-modulation spectroscopy, Chem. Phys. Lett. **495**, 228 (2010).

[8] C. Sciascia, M. Celebrano, M. Binda, D. Natali, G. Lanzani, and J. R. Cabanillas-Gonzalez, Electric field and charge distribution imaging with sub-micron resolution in an organic thin-film transistor, Org. Electron. **13**, 66 (2012).

[9] J. Tsutsumi, S. Matsuoka, I. Osaka, R. Kumai, and T. Hasegawa, Reduced exchange narrowing caused by gate-induced charge carriers in high-mobility donor-acceptor copolymers, Phys. Rev. B **95**, 115306 (2017).

[10] T. Manaka, S. Kawashima, and M. Iwamoto, Charge modulated reflectance topography for probing in-plane carrier distribution in pentacene field-effect transistors, Appl. Phys. Lett. **97**, 113302 (2010).

[11] C. Westermeier, M. Fiebig, and B. Nickel, Mapping of trap densities and hotspots in pentacene thin-film transistors by frequency-resolved scanning photoresponse microscopy, Adv. Mater. **25**, 5719 (2013).

[12] A. R. Davis, L. N. Pye, N. Katz, J. A. Hudgings, and K. R. Carter, Spatially mapping charge carrier density and defects in organic electronics using modulation-amplified reflectance spectroscopy, Adv. Mater. **26**, 4539 (2014).

[13] N. Martino, D. Fazzi, C. Sciascia, A. Luzio, M. R. Antognazza, and M. Caironi, Mapping orientational order of charge-probed domains in a semiconducting polymer, ACS Nano **8**, 5968 (2014).

[14] J. Tsutsumi, S. Matsuoka, T. Yamada, and T. Hasegawa, Gate-modulation imaging of organic thin-film transistor array: Visualization of distributed mobility and dead pixels, Org. Electron. **25**, 289 (2015).

[15] J. Tsutsumi, S. Matsuoka, T. Kamata, and T. Hasegawa, Fast optical inspection of operations of large-area active-matrix backplane by gate modulation imaging, Org. Electron. **55**, 187 (2018).

[16] S. Matsuoka, J. Tsutsumi, T. Kamata, and T. Hasegawa, Microscopic gate-modulation imaging of charge and field distribution in polycrystalline organic transistors, J. Appl. Phys. **123**, 135301 (2018).

[17] S. Matsuoka, J. Tsutsumi, H. Matsui, T. Kamata, and T. Hasegawa, Nanosecond Time-Resolved Microscopic Gate-Modulation Imaging of Polycrystalline Organic Thin-Film Transistors, Phys. Rev. Appl. **9**, 024025 (2018).

[18] B. Blülle, R. Häusermann, and B. Batlogg, Approaching the Trap-Free Limit in Organic Single-Crystal Field-Effect Transistors, Phys. Rev. Appl. **1**, 034006 (2014).

[19] G. Kitahara, S. Inoue, T. Higashino, M. Ikawa, T. Hayashi, S. Matsuoka, S. Arai, and T. Hasegawa, Meniscus-controlled printing of single-crystal interfaces showing extremely sharp switching transistor operation, Sci. Adv. **6**, eabc8847 (2020).

[20] C. Kloc, P. G. Simpkins, T. Siegrist, and R. A. Laudise, Physical vapor growth of centimeter-sized crystals of α-hexathiophene, J. Cryst. Growth **182**, 416 (1997).

[21] J. Takeya, C. Goldmann, S. Haas, K. P. Pernstich, B. Ketterer, and B. Batlogg, Field-induced charge transport at the surface of pentacene single crystals: A method to study charge dynamics of two-dimensional electron systems in organic crystals, J. Appl. Phys. **94**, 9 (2003).

[22] V. Y. Butko, X. Chi, D. V. Lang, and A. P. Ramirez, Field-effect transistor on pentacene single crystal, Appl. Phys. Lett. **83**, 4773 (2003).

[23] W. L. Kalb, T. Mathis, S. Haas, A. F. Stassen, and B. Batlogg, Organic small molecule field-effect transistors with Cytop^{TM} gate dielectric: Eliminating gate bias stress effects, Appl. Phys. Lett. **90**, 092104 (2007).

[24] R. Häusermann and B. Batlogg, Gate bias stress in pentacene field-effect-transistors: Charge trapping in the dielectric or semiconductor, Appl. Phys. Lett. **99**, 083303 (2011).

[25] H. Klauk, Organic thin-film transistors, Chem. Soc. Rev. **39**, 2643 (2010).

[26] H. Chen, Y. Guo, G. Yu, Y. Zhao, J. Zhang, D. Gao, H. Liu, and Y. Liu, Highly π-extended copolymers with diketopyrrolopyrrole moieties for high-performance field-effect transistors, Adv. Mater. **24**, 4618 (2012).

[27] M. Ikawa, T. Yamada, H. Matsui, H. Minemawari, J. Tsutsumi, Y. Horii, M. Chikamatsu, R. Azumi, R. Kumai, and T. Hasegawa, Simple push coating of polymer thin-film transistors, Nat. Commun. **3**, 1176 (2012).

[28] J. Lee, Comment on "Investigation of the device instability feature caused by electron trapping in pentacene field effect transistors" [Appl. Phys. Lett. **100**, 063306 (2012)], Appl. Phys. Lett. **103**, 036101 (2013).

[29] N. J. Hestand, H. Yamagata, B. Xu, D. Sun, Y. Zhong, A. R. Harutyunyan, G. Chen, H.-L. Dai, Y. Rao, and F. C. Spano, Polarized absorption in crystalline pentacene: Theory vs experiment, J. Phys. Chem. C **119**, 22137 (2015).

[30] J. A. Nichols, D. J. Gundlach, and T. N. Jackson, Potential imaging of pentacene organic thin-film transistors, Appl. Phys. Lett. **80**, 2366 (2003).

[31] K. P. Puntambekar, P. V. Pesavento, and C. D. Frisbie, Surface potential profiling and contact resistance measurements on operating pentacene thin-film transistors by Kelvin probe force microscopy, Appl. Phys. Lett. **83**, 5539 (2003).

[32] L. Sebastian, G. Weiser, and H. Bässler, Charge transfer transitions in solid tetracene and pentacene studied by electroabsorption, Chem. Phys. **61**, 125 (1981).

[33] Y. Turkulets and I. Shalish, Franz-Keldysh effect in semiconductor built-in fields: Doping concentration and space charge region characterization, J. Appl. Phys. **124**, 075102 (2018).

[34] M. van Eerden, J. van Gastel, G. J. Bauhuis, P. Mulder, E. Vlieg, and J. J. Schermer, Observation and implications of the Franz-Keldysh effect in ultrathin GaAs solar cells, Prog. Photovolt. Res. Appl. **28**, 779 (2020).

[35] D. C. S. Dumas, K. Gallacher, S. Rhead, M. Myronov, D. R. Leadley, and D. J. Paul, Ge/SiGe quantum confined Stark effect electro-absorption modulation with low voltage swing at $\lambda = 1550$ nm, Opt. Exp. **22**, 16 (2014).

[36] G. Walters, M. Wei, O. Voznyy, R. Quintero-Bermudez, A. Kiani, D.-M. Smilgies, R. Munir, A. Amassian, S. Hoogland, and E. Sargent, The quantu-confined Stark effect in layered hybrid perovskites mediated by orientational polarizability of confined dipoles, Nat. Commun. **9**, 4214 (2018).

[37] L. Zhang, B. Lv, H. Yang, R. Xu, X. Wang, M. Xiao, Y. Cui, and J. Zhang, Quantum-confined stark effect in the ensemble of phase-pure CdSe/CdS quantum dots, Nanoscale **11**, 12619 (2019).

[38] N. I. Ostapenko, V. I. Sugakov, and M. T. Shpak, *Spectroscopy of Defects in Organic Crystals* (Kluwer Academic Publishers, Dordrecht, Boston, London, 1993).